

Decomposition Pathways of the Neutral and Protonated Formamide in Some Lower-Lying Excited States

Huyen Thi Nguyen,[†] Vinh Son Nguyen,[†] Nguyen Tien Trung,[‡] Remco W. A. Havenith,[§] and Minh Tho Nguyen^{*,†}

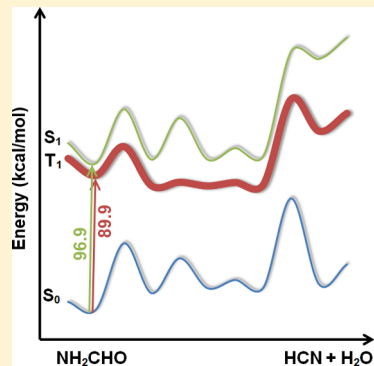
[†]Department of Chemistry, University of Leuven, B-3001 Leuven, Belgium

[‡]Department of Chemistry, Quy Nhon University, Quy Nhon, Vietnam

[§]Theoretical Chemistry, Zernike Institute for Advanced Materials, University of Groningen, NL-9747 AG Groningen, The Netherlands

Supporting Information

ABSTRACT: Unimolecular decompositions of neutral (NH_2CHO) and protonated (NH_3CHO^+) formamide, an active precursor of biomolecules in prebiotic chemistry, are investigated in the ground (S_0) and first triplet (T_1) and singlet (S_1) excited states. Different decomposition channels including the homolytic bond dissociations, dehydration, decarbonylation, dehydrogenation, etc., are explored using coupled-cluster theory (CCSD(T)/CBS method) for both S_0 and T_1 states and RASPT2(18,15)/6-31G(d,p) computations for the S_1 state. On S_1 and T_1 energy surfaces, formamide preferentially follows C–N homolytic bond cleavages forming $\text{NH}_2 + \text{HCO}$ radical pairs. Formation of HCN and HNC from dehydration of neutral and protonated formamide via formimic acid and aminohydroxymethylene isomers has higher energy barriers. A strong stabilization upon triplet excitation of the two latter isomers significantly facilitates the interconversions between isomers, and thus considerably reduces the energy barriers for dehydration pathways. The most probable pathways for HCN and HNC generation are found to be dehydration of formamide in the T_1 state. Dehydration pathways from the neutral S_1 and protonated T_1 forms lead to stable complexes of HCN and HNC with water but are associated with large energy barriers. Overall, in the lower-lying excited states of either neutral or protonated formamide, dehydration is not competitive with homolytic C–N bond cleavages, which finally lead to formation of CO.



1. INTRODUCTION

Formamide (NH_2CHO , FM) is the simplest member of the amide functional group, a basic building unit in proteins. Saladino et al.¹ presented a premise that FM, a ubiquitous molecule in the universe, is an active prebiotic precursor of biomolecules. In this context, photoinduced fragmentations of FM have attracted great interest in part due to the fact that the low molecular weight products of FM partial degradations such as CO, NH_3 , H_2 , HNCO, etc., are obvious intermediates in the prebiotic syntheses.^{1–8}

The decomposition patterns of formamide generating small intermediate molecules have been studied experimentally and theoretically.^{2,3,9} Hydrogen cyanide, HCN, the most studied precursor for biomolecules, and some important precursors for sugars can also be synthesized from formamide.^{9,10} Recently, we explored the decomposition pathways of FM on its ground singlet state (S_0) using high accuracy coupled-cluster theory methods allowing a consistent comparison between different channels.² The multistep decarbonylation involving a carbene isomer of FM (aminohydroxymethylene, H_2NCOH) has a slightly lower energy barrier than the one-step pathway. Both CO elimination channels were found to be more favorable than the one-step H_2 elimination. In the multistep dehydration

processes forming HCN and HNC species, H_2O eliminations are the rate-determining steps involving high energy barriers of 73.6 and 83.7 kcal/mol. The water molecules formed from this step could in turn act as a bifunctional catalyst reducing significantly the energy barrier of the dehydration of FM.¹¹ Different reaction pathways that do not involve an initial dehydration of FM were also explored in detail.¹² These pathways involving instead multiple participation of FM molecules lead to formation of purine and adenine with significantly lower energy barriers.

Photodecomposition of FM in low-temperature matrixes revealed two main channels.³ In Ar matrixes, irradiation of FM excites the molecule to its first excited singlet S_1 state where the C–N bond dissociates to form a radical pair $\text{HCO} + \text{NH}_2$. The subsequent dissociation of the HCO radical rapidly releases H^\bullet , which is immediately transferred to the NH_2 radical to form NH_3 . However, in Xe matrixes, the effect of the external heavy atom induces an intersystem crossing from the S_1 to the first

Received: June 7, 2013

Revised: July 25, 2013

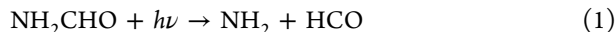
Published: July 26, 2013



triplet T₁ state energy surface, leading to a dehydrogenation giving HNCO + H₂ as main products, instead of NH₃ + CO.

The photolysis of FM was also investigated by laser-induced fluorescence spectra of H(²S) at 205 nm.⁵ It was concluded that bond dissociations took place on the T₁ energy surface with energy barriers of 18.1 and 39.4 kcal/mol for H₂NCO + H and HNCHO + H product channels, respectively.

Five reaction channels 1–5 upon photoexcitation of FM proposed by Boden et al.¹³ have theoretically been studied at different levels of theory.^{4,6}



In addition to these product channels, a trace amount of HCN was also detected during photolysis when an unfiltered mercury arc is used as a light source.¹³ Of these reaction channels, the C–N bond cleavage channel (1) is found to be the most favorable channel on the S₁ surface.^{4,6,13} Dynamics simulations starting on the S₁ state energy surface constructed at the SA-CASSCF(10,8)/6-31G(d) level showed that the major decomposition channel is C–N dissociation with an average decay time to the S₀ state of ~420 fs.⁶ The C–H bond dissociation channel was observed in only 4% of the trajectories, whereas in 16% of trajectories, the FM molecule remained in the minimum of S₁ surface with 5% going back to the nondissociated FM ground state.

The surface hopping dynamics calculations were also used to probe the effects of protonation on photodissociation processes in FM.⁸ Photodeactivation processes from the S₁ state of the protonated FM were also investigated. The C–N (major) and C–O (minor) bond dissociation channels were found in the O-protonated FM, whereas in the N-protonated FM, only the C–N bond cleavage was observed with much longer lifetimes. This study⁸ also showed the existence of other deactivation processes in N-protonated FM because 55% of trajectories remained nondissociated and nondeactivated until the end of the simulation time (1000 fs).

The energy difference between both N- and O-protonated forms of FM in the S₀ state has extensively been predicted using different levels of theory.^{14–20} The O-protonated form is ~13–26 kcal/mol more stable than N-protonated isomer in the ground S₀ state, but such a difference is reduced to 6 kcal/mol²¹ in the excited S₁ state. Two reaction channels for O-protonated isomer and one reaction channel for N-protonated isomer on the S₀ surface were theoretically studied by Lin et al. at the MP2/6-31G(d,p) level.¹⁵ The O-protonated form could either rearrange to its N-protonated isomer, which undergoes subsequently a H-transfer forming the NH₄⁺ + CO products, or directly follow a H-transfer forming dehydration [HCN]⁺ + H₂O products. An alternative path for the N-protonated FM was also mentioned without determining the relevant transition structure. This path yields [HCO]⁺ + NH₃, which are however 64.5 kcal/mol higher in energy than the [NH₄]⁺ + CO counterparts.

A more complete potential energy surface of protonated FM was constructed by Tortajada et al.¹⁸ at the G2 level leading to different products, [NH₄]⁺ + CO, NH₃ + [HCO]⁺, H₂O +

[NH₂C]⁺, NH₃ + [COH]⁺, H₂O + [HCN]⁺, and OH + [HCNH]⁺. The lowest possible pathway turns out to be an initial rearrangement of the O-protonated form yielding its N-protonated isomer followed by H-transfer finally giving rise to NH₄⁺ + CO. This overall corresponds to a decarbonylation of the protonated FM.

In relation to our continuing theoretical study of formamide prebiotic chemistry,^{2,11,12} we set out to investigate the reaction channels leading to decompositions of the neutral and protonated FM, not only in the ground electronic state but also in the excited triplet T₁ and singlet S₁ states.

In the T₁ state, the neutral FM undergoes homolytic fissions forming NH₂ + HCO, H + H₂NCO, and H + HNCHO pairs of radicals. These high energy products are not readily formed from the ground S₀ state. One of these homolytic pathways results in formation of CO with a low energy barrier. We thus re-explore the decarbonylation [NH₄]⁺ + CO and dehydration H₂O + [HNCH]⁺ product channels previously reported by Tortajada et al.¹⁸ Some new decomposition channels of protonated FM on the S₀ surface including the dehydrogenation and hydronium (H₃O⁺) elimination are also identified. The protonated FM mostly undergoes in the T₁ state homolytic reactions yielding a variety of small products: CO, H[•], [NH₃]^{•+}, [H₂NCO]⁺, etc.

Of particular interest are the pathways occurring on the excited S₁ state. Homolytic dissociation channels (1)–(3), the decarbonylation (4), the interconversions of FM and its isomers, and the dehydration of these isomers forming HCN and HNC products are studied. For homolytic bond dissociation channels, only the first step of each channel, which is the homolytic bond dissociation of CN/CH/NH bond, is studied. Different possible subsequent reactions of the products of these first steps were investigated in detail in a recent paper.⁹

2. COMPUTATIONAL METHODS

Geometries of the stationary points on the ground S₀ and lowest-lying T₁ states of formamide can be determined using the single determinant Hartree–Fock-based methods such as second-order perturbation (MP2) and coupled-cluster (CC) theories, and density functional theory (DFT). On the contrary, geometries of the excited singlet S₁ and S₂ states need to be determined using multiconfigurational approaches. Thus, two different sets of quantum chemical computations are carried out.

2.1. Multiconfigurational Wave Function Computations. To obtain a set of consistent results on geometries and energies, the structures of FM in the S₀, S₁, S₂, and T₁ electronic states are fully optimized using the multiconfigurational method with the restricted active space self-consistent field (RASSCF) technique,^{22,23} in conjunction with the 6-31G(d,p) basis set. For the singlet S₀, S₁, and S₂ states, the state-averaged RASSCF method is used with three states weighted equally. Meanwhile, the ground S₀ and triplet T₁ FM geometries are optimized with the state-specific RASSCF method to determine the optimized geometry of the T₁ FM, and the energy difference between both T₁ and S₀ states.

The frontier orbitals of FM include the π(HOMO–1), n(HOMO), and π*(LUMO). The singlet S₁ state is basically formed following the n → π* excitation, whereas the S₂ state arises from the π → π* excitation. The triplet T₁ state can be considered as generated from the n → π* transition.

In general, the RASSCF technique divides the active space into three subspaces called *RAS1*, *RAS2*, and *RAS3*. The *RAS1* includes doubly occupied orbitals, whereas the *RAS3* contains unoccupied orbitals generated from the Hartree–Fock reference determinant. A number of holes and electrons can be allowed in *RAS1* and *RAS3*, respectively, to allow electron excitations between three subspaces. The *RAS2* subspace is treated in a manner analogous to that of the active space in a complete active space SCF (CASSCF) calculation. Because of this partition, the RASSCF approach is greatly less computational demanding as compared to a full CASSCF and thus allows the calculations with larger active spaces to be achieved. In this work, the active spaces including 18 electrons and 15 orbitals are chosen and distributed in two subspaces, *RAS2* and *RAS3*, with the number of orbitals in *RAS2*:*RAS3* being 10:5. The maximum of two electrons are allowed to excite to the *RAS3* subspace.

Harmonic vibrational frequency analyses are performed at the RASSCF level to confirm the nature of the stationary structures. Single point second-order perturbation theory RASPT2²⁴ calculations are subsequently carried out at the RASSCF optimized geometries to determine the dynamic correlation energies. All of the calculations are performed using the MOLCAS 7.6 programs.

2.2. The Ground and Triplet States of Neutral and Protonated Formamide. To construct the potential energy surfaces of FM and its protonated form in both ground S_0 and lowest-lying T_1 states that can be treated by single reference methods, the Møller–Plesset perturbation theory at the second-order with the correlation-consistent polarized plus diffuse functions aug-cc-pVQZ basis set is used to optimize the geometries and to evaluate zero-point vibrational (ZPE) corrections to the energies of all equilibrium and transition structures considered. Final geometrical parameters of the relevant stationary points are then recalculated using the same MP2 method but with a larger aug-cc-pVTZ basis set. The optimized MP2/aug-cc-pVTZ geometries are subsequently used for a series of single point coupled-cluster theory CCSD(T) calculations with the aug-cc-pVnZ with $n = D, T, Q$ basis sets. Total energies obtained from these single point calculations are then used to extrapolate the total coupled-cluster energies to the complete basis set limit (CBS) using the expression as follows:²⁵

$$E(n) = E(\text{CBS}) + B \exp[-(n - 1)] + C \exp[-(n - 1)^2]$$

where $E(n)$ and $E(\text{CBS})$ are the CCSD(T)/aug-cc-pVnZ and CCSD(T)/CBS energies, respectively.

Relative energies between the stationary points on each potential energy surface are calculated using extrapolated CCSD(T)/CBS energies and ZPE corrections obtained at the MP2/aug-cc-pVQZ level. All electronic structure calculations in this series are performed using the Gaussian 09 suite of program.²⁶

3. RESULTS AND DISCUSSION

In following the convention of a previous theoretical paper on decomposition pathways of protonated FM on the S_0 surface,¹⁸ the isomers FM ($\text{NH}_2\text{CH}=\text{O}$), formimic acid ($\text{NH}=\text{CH}-\text{OH}$), and aminohydroxymethylene (NH_2COH) are denoted as 1, 2, and 3, respectively. The letter H or R is added to the name of each of these compounds to indicate if it is in the protonated or radical form, respectively. Different protonated and radical

forms of the same compound can be distinguished from each other by adding symbol superscripts, for example, 1H , $1\text{H}'$, $1\text{H}''$, 1H^* , 2R , $2\text{R}'$, etc. The transition state structures are denoted as $\text{ts-A},\text{B}$ where A and B are the two energy minima being connected by this transition structure (ts). The letters S_1 , S_2 , and T_1 are also added to a label to indicate the electronic state, for example, $1\text{-S}1$, $1\text{-S}2$, etc. For the S_0 FM calculated by the RASSCF method, we use the labels 1SA and 1SS for geometries obtained from state-average and state-specific RASSCF calculations, respectively.

The potential energy surface of the FM ground state has been explored in much detail at the CCSD(T)/CBS level in a previous study.² Let us briefly mention that of the possible decomposition pathways including the dehydration, decarbonylation, and dehydrogenation, the multistep dehydration yielding HCN turns out to be slightly favored, but the associated energy barrier is high (>75 kcal/mol). For the sake of consistency, we use the RASPT2 relative energies in the following discussion of the excited states of FM.

3.1. Excited States of Neutral Formamide. **3.1.1. Optimized Geometries.** The RASSCF optimized structures of FM 1 in the S_0 , S_1 , S_2 , and T_1 states are plotted in Figure 1. The

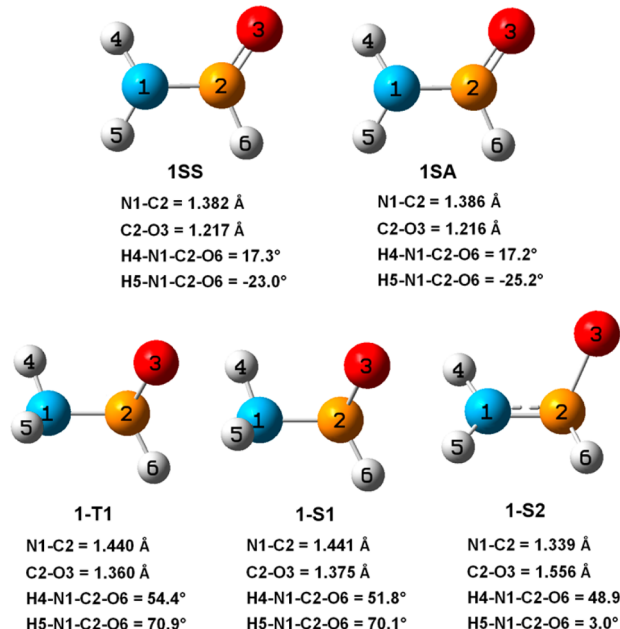


Figure 1. Optimized structures of formamide in the S_0 (1SS, 1SA), S_1 (1-S1), S_2 (1-S2), and T_1 (1-T1) states obtained using RASSCF-(18,15)/6-31G(d,p) calculations.

planarity of FM has been a subject of strong debate. Fogarasi et al.²⁷ reported massive electron correlation computations focusing on its equilibrium geometry and the rotational barrier around the C–N bond. The authors listed a large number of experimental and theoretical works on the planarity of FM in the S_0 state in which high level computations appear to lead to nonplanarity. The difference between planar and nonplanar is however negligible, and 1 can be considered as an “essentially” planar molecule.³ However, it was also proven that the nonplanar S_0 geometry yielded a slightly lower vertical excitation energy as compared to the excitation from planar FM.²⁸ The reduction in the vertical $S_0 \rightarrow S_1$ transition energy amounts to 3.7 kcal/mol if 1 is distorted out of the plane by ~12°.

In the present work, both state-specific and state-average RASSCF calculations yield nonplanar structures with a slightly pyramidal NH_2 moiety. With an imaginary frequency the planar structure is, as expected, a transition structure for the inversion of NH_2 group. Although the difference between **1SS** and **1SA** optimized structures is very small, there is a significant gap in the calculated RASSCF energies between them, with **1SS** being 10.5 kcal/mol more stable than **1SA**. This energy gap is reduced to a more acceptable value of 3.0 kcal/mol at the RASPT2 level.

Equilibrium structures of **1-S1**, **1-S2**, and **1-T1** are greatly distorted from the planar form (cf., Figure 1). These structures are in agreement with the previously reported ones for **1-S1** and **1-T1** having the pyramidal NH_2 and HCO groups, and **1-S2** species having a pyramidal HCO and a planar NH_2 groups.²⁹ The $n \rightarrow \pi^*$ excitation results in elongations of C–O and C–N bonds. The C–O bond lengths of **1-S1** and **1-T1** increase by 0.16 and 0.14 Å, respectively, upon excitation. The effect of excitation on C–N bond length is smaller with increases of 0.05 and 0.06 Å for **1-S1** and **1-T1**.

The optimized geometry of **1-S2** shows a significant elongation of the C–O bond, while the C–N bond is getting slightly shorter as compared to the S_0 FM. However, dynamics simulations starting from the $\pi \rightarrow \pi^*$ state showed that a majority of the deactivation trajectories of FM after excitation to the S_2 state is the C–N dissociation, and only 13% of all observed events represent C–O bond cleavage.⁶ This suggests that after being excited to the S_2 state, only a small portion of the excited molecules can reach the minimum of the S_2 surface with the elongated C–O bond that ultimately facilitates C–O bond dissociation.

3.1.2. Excitation Energies. Calculated vertical and adiabatic excitation energies of FM at both RASSCF and RASPT2 levels are listed in Table 1. The RASSCF method consistently

133.2,^{7,31,32} 170.6–179.2,^{7,31,32} and 120.8–123.1 kcal/mol^{28,33} for $S_0 \rightarrow S_1$, $S_0 \rightarrow S_2$, and $S_0 \rightarrow T_1$ excitations, respectively.

The adiabatic excitation energies ($E_{\text{Ex,a}}$) are found to be much smaller than the corresponding vertical values. The relaxation energies of FM on the S_1 , S_2 , and T_1 surfaces predicted at RASPT2 level amount to 31.0, 37.6, and 30.2 kcal/mol, respectively. Dynamical correlation significantly increases the energy difference between the S_1 and T_1 equilibrium structures. RASSCF calculations yield a very small energy gap of 2.3 kcal/mol, while the RASPT2 gap is 8 kcal/mol in favor of the T_1 state.

Previous CASSCF and CASPT2 calculations with a smaller active space showed an extremely small energy gap of 0.6 kcal/mol between the S_1 and T_1 equilibrium structures.⁴ The variance between our RASPT2 and previous calculated data arises from a dissimilarity in the predicted T_1 minimum energy geometry. While the S_1 minimum energy geometry is very close to previous predictions with differences in the range of 2.9–3.6 kcal/mol,^{4,6,21} the T_1 minimum energy is smaller by 8.9–10.3 kcal/mol.^{2,4,5} The RASPT2 energy of **1SS** is, as mentioned above, 3.0 kcal/mol higher than **1SA**, while the RASSCF energy of the former is 10.5 kcal/mol lower. Such a mismatch between both calculated energies for the S_0 FM could account for the larger $S_0 \rightarrow T_1 E_{\text{Ex,a}}$ value, as compared to $S_0 \rightarrow S_1 E_{\text{Ex,a}}$ at the RASSCF level, and the small $S_0 \rightarrow T_1 E_{\text{Ex,a}}$ value at the RASPT2 level.

3.1.3. Reaction Pathways on the S_1 Energy Surface. Different dissociation reaction pathways starting from **1-S1** are presented in Figure 1 with relative energies of all species considered obtained at the RASPT2 level.

The C–N dissociation channel (1) has the lowest energy barrier of 15.5 kcal/mol. This value lies between those predicted by Antol et al.⁶ and Liu et al.⁴ Because the products with either $\text{NH}_2\text{-S1}$ radical or HCO-S1 radical lie at 14.4 and 14.9 kcal/mol above the **ts-1,P-S1**, after CN dissociation the system would preferentially jump to the S_0 surface via internal conversion forming $\text{NH}_2 + \text{HCO}$ radical pair in the S_0 state. The very unstable HCO radical immediately dissociates giving $\text{CO} + \text{H}$. The energy of the $S_0 \text{ NH}_2 + \text{HCO}$ radical pair is located at 6.2 kcal/mol below the optimized **1-S1** species, and thus 90.7 kcal/mol above the optimized **1-SA**. This RASPT2 energy of the $\text{NH}_2 + \text{HCO}$ radical pair is in agreement with the reported experimental value of 90.4 kcal/mol.⁴ CCSD(T)/CBS computations predicted less stable $\text{NH}_2 + \text{HCO}$ products with an energy of 98.0 kcal/mol with respect to **1**.²

The C–H bond dissociation channel (2) has a much higher energy barrier than the C–N with a RASPT2 value of 35.7 kcal/mol. This value is quite close to the previous CASSCF-(10,8)/6-31G(d) energy barrier of 36.2 kcal/mol.⁶ The value obtained at the CASPT2(8,7)/6-31G(d) level of 41.3 kcal/mol is slightly higher.⁴ The $\text{H} + \text{R1-S1}$ products lie 28.2 kcal/mol above **ts-1,R1-S1**. The energy of the $S_0 (\text{H} + \text{R1})$ radical pair is close to the $S_0 (\text{NH}_2 + \text{HCO})$ products with an energy of 90.6 kcal/mol higher than **1-SA**. Although this value is in agreement with the CCSD(T)/CBS result of 92.7 kcal/mol,² experiment showed much more stable ($\text{H} + \text{R1}$) products with a relative energy of 71.7 kcal/mol with respect to **1** (FM).⁴

Two N–H dissociation channels (3) are studied in the present work. The energy barriers of both pathways of 32.3 and 35.9 kcal/mol are quite close to that of C–H bond cleavage. Although the difference in energy barriers between both N–H dissociations is small, the stabilities of the two resulting sets of products are clearly different from each other, with **R2-S1** being

Table 1. Vertical ($E_{\text{Ex,v}}$) and Adiabatic ($E_{\text{Ex,a}}$) Excitation Energies in kcal/mol of Formamide Obtained at the RASSCF/6-31G(d,p) and RASPT2/6-31G(d,p)//RASSCF/6-31G(d,p) Levels

	$E_{\text{Ex,v}}$			$E_{\text{Ex,a}}$	
	RASSCF	RASPT2	exp. ³⁰	RASSCF	RASPT2
S_1	133.0	127.9	133.7	98.4	96.9
S_2	196.6	183.1	170.6	152.1	145.5
T_1	134.1	119.1	119.9	100.7	88.9

predicts larger excitation energies than the RASPT2 counterpart. Although the calculated RASSCF $S_0 \rightarrow S_1$ vertical excitation energy ($E_{\text{Ex,v}}$) is extremely close to the experimental value,³⁰ the theoretical data at this level for the $S_0 \rightarrow S_2$ and $S_0 \rightarrow T_1$ excitations are considerably overestimated by an amount of 26.0 and 14.2 kcal/mol, respectively. With the inclusion of dynamical correlation, the predicted $S_0 \rightarrow S_2$ and $S_0 \rightarrow T_1 E_{\text{Ex,v}}$ values approach much closer to the experimental ones. However, the difference between experimental and theoretical $S_0 \rightarrow S_2 E_{\text{Ex,v}}$ remains large with the calculated value being overestimated by 12.5 kcal/mol.

It should be noted that the RASSCF method predicts the $S_0 \rightarrow T_1 E_{\text{Ex,v}}$ value to be slightly larger than the $S_0 \rightarrow S_1 E_{\text{Ex,v}}$, while the ordering is reversed by RASPT2 results. Overall, our results are in agreement with several recently reported theoretical $E_{\text{Ex,v}}$ values, which are in the ranges of 131.6–

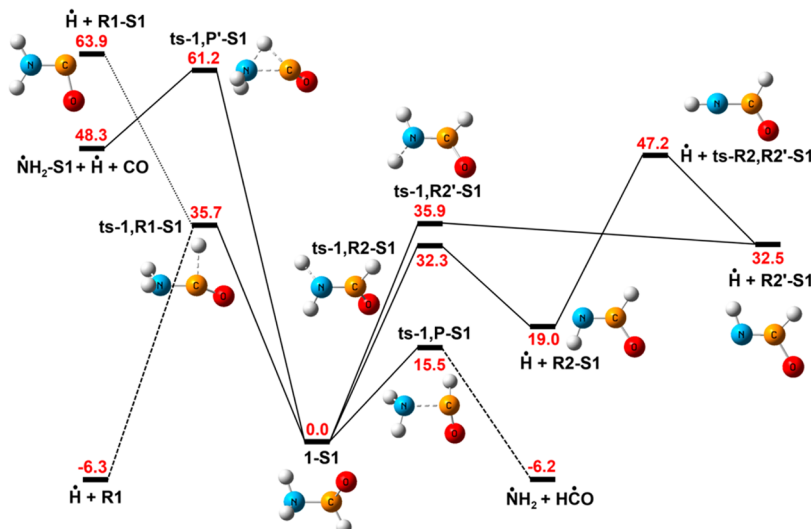


Figure 2. Schematic energy profiles illustrating the homolytic dissociation pathways of formamide in the S_1 state. RASPT2 relative energies are given in kcal/mol.

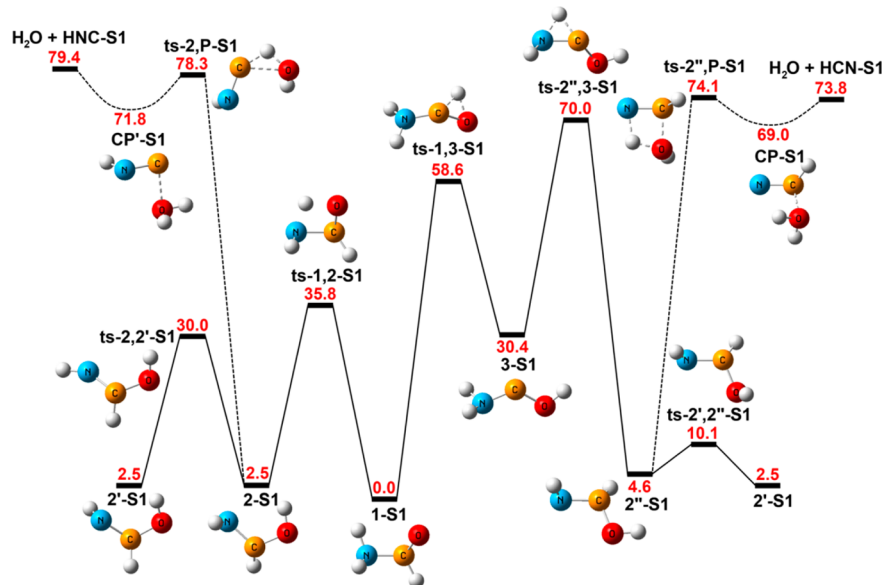


Figure 3. Schematic energy profiles illustrating the interconversions between isomers and the dehydration of formamide in the S_1 state. RASPT2 relative energies are given in kcal/mol.

13.5 kcal/mol more stable than its $R2'-S1$ counterpart. The previous theoretical value⁶ for the barrier of the N–H dissociation channel forming $R2-S1$ product is very close to our RASPT2 results, with a difference of less than 1 kcal/mol. The difference in energy between both products is reduced from 13.5 kcal/mol in the S_1 to 3.1 kcal/mol in the S_0 state. The corresponding products $H + R2$ and $H + R2'$ of the two N–H dissociation channels in the ground S_0 state are located at 109.7 and 112.8 kcal/mol above $1-S_A$, respectively. These values are comparable to the reported experimental value of 104.5 kcal/mol.⁴

The decarbonylation of $1-S1$ via $ts-1,P'-S1$ is also displayed in Figure 2. The transition structure $ts-1,P'-S1$ for this reaction is located at much higher than the TSs for the dissociations, with a RASPT2 relative energy of 61.2 kcal/mol. The latter is in agreement with the previous value of 60.9 kcal/mol at CASPT2(8,7)/6-31G(d).⁴ The set of products with $CO-S1$

lies much higher than the transition state $ts-1,P'-S1$, and thus is not presented here.

The excited NH_3 molecule dissociates yielding NH_2-S1 and H radical. This set of products is located at 48.3 kcal/mol above $1-S1$.

Other reaction pathways are possible via the transformation from $1-S1$ to formimic acid and carbene isomers. Relative stabilities of different isomers of FM on the S_1 surface (cf, Figure 3) are quite similar to those on the S_0 surface.² The isomer $3-S1$ is found at 30.4 kcal/mol above $1-S1$, whereas different rotamers of formimic acid are 2.5–4.6 kcal/mol less stable than $1-S1$. The barrier for conversion of $1-S1$ to $3-S1$ is much larger than the barrier connecting $1-S1$ and $2-S1$. The latter barrier being 132.7 kcal/mol higher than 1 is close to the $S_0 \rightarrow S_1 E_{Exy}$ value. Therefore, the excited FM molecules are likely to have enough internal energy to overcome this barrier forming $2-S1$. The $2-S1$ species needs to overcome a lower

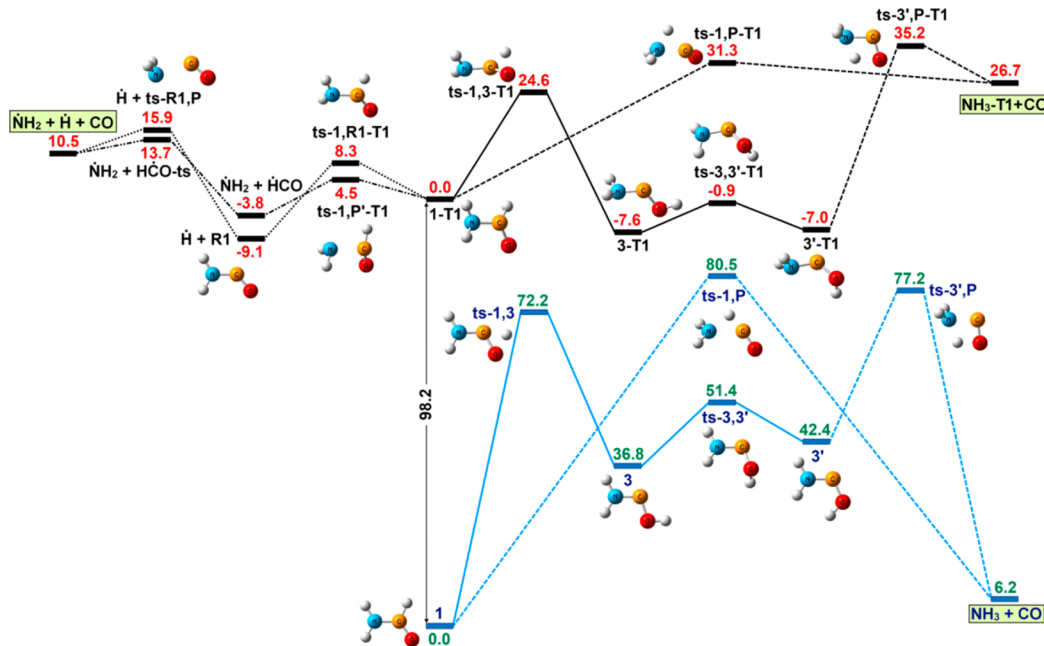


Figure 4. Schematic potential energy profiles illustrating decarbonylation reactions of formamide in both S₀ and T₁ states. CCSD(T)/CBS + ZPE energies (kcal/mol) are relative to **1** on the S₀ surface and to **1-T1** on the T₁ surface.

barrier height of 27.5 kcal/mol to form 2'-S1 rotamer, and the 2"-S1 rotamer is easily formed from the latter with a barrier of 7.6 kcal/mol.

Formation of HCN and HNC in the S₁ state is also possible via dehydration of the 2"-S1 and 2-S1 species, respectively. However, these channels are characterized by very large energy barriers of 69.5 kcal/mol for formation of HCN-S1 and of 75.8 kcal/mol for formation of HNC-S1. The associated products are also high-lying species, with the water complexes being more favorable than the separated ones.

In general, the topography of the S₁ surface is similar to that of the S₀ surface with FM (**1** and **1-S1**) being the most stable isomer and carbene (**3** and **3-S1**) being the least stable one. The similarity can clearly be observed by overlapping two surfaces (cf., Figure S1); the interconversions of FM S₁ follow those of FM S₀ with the relative energies of related S₁ species being consistently lower. In both energy surfaces, HCN (or HCN-S1) is formed from dehydration of formimic acid isomer 2" (or 2"-S1). However, different from HNC S₀ formation, HNC-S1 is formed from 2-S1 instead of 3-S1.

3.2. Triplet Excited State of Neutral Formamide.

3.2.1. Formamide and Its Isomers in the First Triplet Excited State. The vertical and adiabatic S₀ → T₁ excitation energies of FM have extensively been evaluated at different levels of theory.^{4,28,33–36} The calculated vertical excitation energies are in the range of 120.8–124.3 kcal/mol, which are in good agreement with the experimental values of 122.2 kcal/mol reported by Staley et al.³⁷ and of 120.0 kcal/mol by Gingell et al.³⁰ The vertical excitation energy of 123.6 kcal/mol obtained from our CCSD(T)/CBS calculation lies within the range of reported theoretical data, and thus also close to experiment. When FM is allowed to geometrically relax on the T₁ surface, the excitation energy decreases from 123.6 to 98.2 kcal/mol (CCSD(T)/CBS). The latter is very close to that of 99.2 kcal/mol reported by Liu and co-workers.⁴ Such a difference between vertical and adiabatic excitation energies indicates a large distortion of the molecular skeleton upon excitation to the

T₁ state. The MP2/aug-cc-pVTZ **1-T1** structure is substantially distorted from the planar S₀ structure along with elongations of C–N and C–O bond distances by an amount of 0.06 and 0.13 Å, respectively. These bond length variations are in agreement with RASSCF values. The relative orientation between HCO and NH₂ fragments of our optimized **1-T1** slightly differs from Liu's structure.⁴ However, further comparisons of reaction barriers indicate that our structure leads to lower energy barriers for the direct decarbonylation and homolytic reactions, whereas for other channels, the energy barriers are very close to each other.

As compared to FM, the formimic acid **2** and carbene **3** isomers exhibit much lower adiabatic excitation energies. It is remarkable that on the T₁ surface, **3-T1** becomes the most stable isomer at 7.6 kcal/mol lower than **1-T1**. The energies of different rotamers of formimic acid **2-T1** are very close to that of **3-T1** and consistently more stable than **1-T1**. Such a reversed energy ordering was also observed for the ionized form of FM and its isomers in which the carbene radical cation becomes the most stable one.³⁸ Similar to **1-T1**, structures of **2-T1** and **3-T1** are also substantially rotated out of the plane. Such distortions of the geometries of **1-T1**, **2-T1**, and **3-T1** significantly facilitate the interconversions between them (cf., Figure 4). The barrier for conversion between **1-T1** and **2-T1** is reduced by 24.8 kcal/mol as compared to the amount on the S₀ surface. For the conversion between **1-T1** and **3-T1**, the triplet excitation induces an even stronger effect, with a reduction of 47.6 kcal/mol on energy barrier. Rearrangements between different rotamers of carbene **3-T** and formimic acid **2-T** also become more favored with lower barrier heights. Because it was proven that multistep decarbonylation and dehydration involve the carbene and formimic acid isomers,² such easy transformations between them and formamide would be beneficial for these reaction pathways.

3.2.2. Decomposition Pathways of Formamide in the First Triplet Excited State. On the T₁ potential energy surface, several pathways are open leading to formation of CO: (i) one-

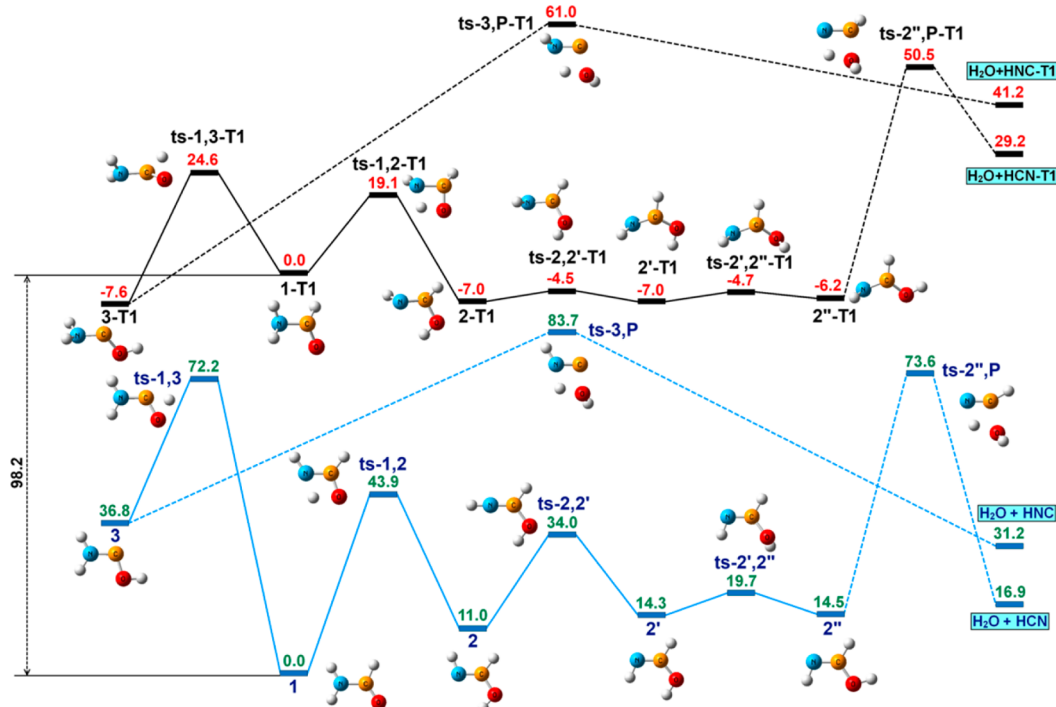


Figure 5. Schematic potential energy profiles illustrating dehydration reactions of formamide in both S_0 and T_1 states. CCSD(T)/CBS + ZPE energies (kcal/mol) are relative to **1** on the S_0 surface and to **1-T1** on the T_1 surface.

step reaction via **ts-1,P-T1**, (ii) multistep channel via **3-T1** isomer, (iii) multistep channel via C–N homolytic bond dissociation, and (iv) multistep reaction via C–H homolytic bond dissociation. The potential energy profiles of these reaction pathways are schematically illustrated in Figure 4, along with the available corresponding reaction pathways on the S_0 surface for the purpose of comparison. It should be noted that energies of different structures on both surfaces are relative to the energy of FM as reference in each surface.

Formation of CO on T_1 preferentially proceeds through a homolysis of the C–N bond yielding $\text{NH}_2 + \text{HCO}$ radical pair, followed by further elimination of H atom from the latter. The homolytic pathway (iv) via carbamyl radical (NH_2CO , R1) is highly competitive with the lowest pathway because the barrier height of this pathway is only 2.2 kcal/mol higher. The NH_2CO radical was experimentally observed in high-temperature photolysis of FM vapor, which further dissociates to form CO and releases the NH_2 radical.³⁹

Although the one-step (i) and multistep (ii) pathways are less favorable as compared to the bond homolytic cleavages, their energy barriers are consistently much lower than those on the S_0 surface. Reduction in energy barrier of (i) can be understood by examining the variations of the geometrical parameters in going from reactants to transition structures. The $C_1\text{--}N_3$ distance of **ts-1,P-T1** is 1.57 Å, being ~0.30 Å shorter than that of **ts-1,P**. Because of the elongation of the $C_1\text{--}N_3$ bond length upon triplet excitation, the TS is close to **1-T1** with only 0.15 Å difference in the $C_1\text{--}N_3$ bond length. Meanwhile, there is a large variation of 0.50 Å in the $C_1\text{--}N_3$ bond length in going from **1** to **ts-1,P**. However, for the multistep channel (ii), the lowering of the T_1 energy barrier is mostly due to a significant stabilization of **3-T**, the carbene isomer following triplet excitation. Although the rate-determining step, which is the intramolecular H transfer of **3'-T1** to form the final products ($\text{NH}_3\text{-T1} + \text{CO}$), has an energy barrier

of 42.2 kcal/mol, being 7.4 kcal/mol larger than that on the S_0 surface, the overall reaction barrier of this channel in the T_1 state is still substantially lower by an amount of 40.0 kcal/mol.

Our predicted energies of the transition structures **ts-1,P-T1**, **ts-1,P'-T1**, and **ts-1,R1-T1** are 13.7, 8.9, and 12.2 kcal/mol lower than the corresponding energies from a previous calculation.⁴ We recalculated the energies of **ts-1,P-T1** and **ts-1,R1-T1** using Liu's structures⁴ as starting geometries in an attempt to figure out the reason for such differences. These structures are denoted hereafter as **ts-1,P-T1-Liu** and **ts-1,R1-T1-Liu**. The MP2/aug-cc-pVQZ optimized geometry of **ts-1,P-T1-Liu** has the $C_1\text{--}N_3$ distance of 2.17 Å, which lies between our value of 1.57 Å and Liu's CASSCF value of 2.44 Å. The **ts-1,R1-T1-Liu** geometry also has a shorter $C_1\text{--}H_4$ distance as compared to that of Liu's CASSCF result, but in this case, this $C_1\text{--}H_4$ distance is close to our value. CCSD(T)/CBS relative energies for **ts-1,P-T1-Liu** and **ts-1,R1-T1-Liu** turn out to be closer to our RASPT2 values than to those of Liu.

For the direct decarbonylation reaction, the difference in energy barrier is reduced from 13.7 to 1.6 kcal/mol when comparing our barrier with Liu's CASSCF and **ts-1,P-T1-Liu** values, respectively. In the C–H homolytic reaction, the barrier difference is also reduced from 12.2 to 5.9 kcal/mol. From these observations, we would suggest that the differences in our present TSs and Liu's CASSCF TSs are mostly due to an inherent difference in the levels of calculation. MP2/aug-cc-pVTZ calculations tend to predict TSs with shorter distance between the two involving atoms of the broken bonds. This can be explained by the fact that CASSCF calculations take the σ^* orbitals of the corresponding breaking bonds into account, whereas MP2 calculations do not.

Two possible pathways leading to FM dehydration on the T_1 surface are presented in Figure 5. The first pathway involving formimic acid isomer **2-T1** gives rise to formation of HCN in the T_1 state. The second one forms HNC also in the T_1 state

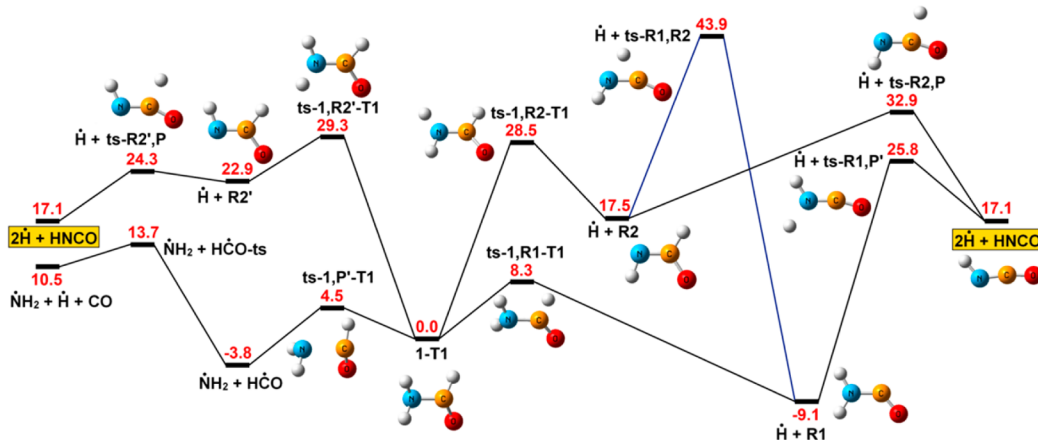


Figure 6. Schematic potential energy profiles describing the reaction pathways of formamide yielding isocyanic acid (HNCO) in the T_1 state. CCSD(T)/CBS + ZPE energies (kcal/mol) are relative to 1-T1.

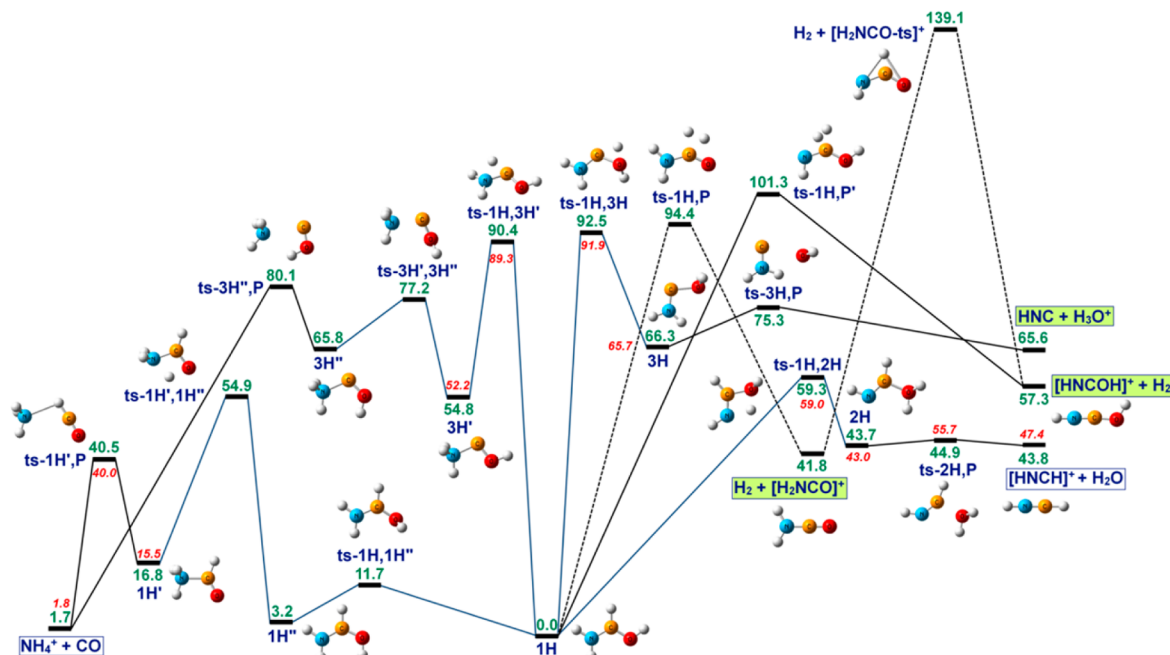


Figure 7. Schematic potential energy profiles of the reaction pathways of protonated formamide in the S_0 state. CCSD(T)/CBS + ZPE energies (kcal/mol, green color) are relative to 1H. G2 relative energies taken from ref 18 are given in red.

via the carbene isomer 3-T1. The overall reaction barriers of both T_1 pathways are lower than those on the S_0 surface by an amount of ~ 23 kcal/mol. Similar to the decarbonylation, the energy barrier associated with the rate-determining step in the second T_1 pathway is actually higher than that on the S_0 surface, but the overall reaction barrier remains lower, due to a strong stabilization of the carbene isomer 3-T1.

However, for the pathway via T_1 formimic acid, the barrier of the rate-determining step is slightly lower than the corresponding S_0 value. This is again due to a stabilization of the formimic acid following triplet excitation, but it is now less profound than that of carbene. The adiabatic triplet excitation energy of 2 is close to that of formamide, being 80.2 kcal/mol (the difference between 2 and 2-T1), whereas the adiabatic singlet-triplet gap of 3 is only 53.8 kcal/mol (the difference between 3 and 3-T1). From comparison between two possible T_1 pathways, the path leading to the $H_2O + HCN\text{-}T1$ set of products is more favored than the one leading to $H_2O + HNC\text{-}T1$. The difference in

both reaction barriers is ~ 10 kcal/mol, which is similar to that on the S_0 surface.

Formation of isocyanic acid (HNCO) on the T_1 surface is now a two-step process in which the first step involves a X–H homolytic bond dissociation (X = C, N) (cf., Figure 6). The radicals R1, R2, and R2' forming from the first step subsequently dissociate to form HNCO. The H atom released in the first step can in turn act as the reactant in the second step to produce the molecular H_2 by radical recombination.

Among the three possible homolytic dissociations, the C–H bond breaking results in the most stable radical R1, which is at 9.1 kcal/mol below 1-T1. Pathway via R1 is also the lowest possible pathway leading to formation of HNCO in which the energy barrier of the rate-determining step amounts to 25.8 kcal/mol. This barrier is much higher than that of decarbonylation, indicating that HNCO (and thus H_2) is a minor product. This is in agreement with a previous experimental report on high-temperature photolysis of FM vapor in which

NH_3 and CO were identified as major products, and H_2 a minor one.³⁹

The N–H bond dissociations yield two different isomers of HNCHO with **R2** being slightly more stable than **R2'**. However, the overall energy barrier of the pathway via **R2** is found to be actually larger than that via **R2'**. In the latter, the N–H bond breaking is the rate-determining step with an energy barrier of 29.3 kcal/mol, whereas the rate-determining step of the former pathway is the second step with a still large barrier of 32.9 kcal/mol. Transformation of **R2** to **R1** followed by dissociation of **R1** to form HNCO has a very high barrier as compared to the direct HNCO formation from **R2**, and thus is not favored.

3.3. Protonated Forms of Formamide and Their Decompositions. FM protonation has extensively been investigated using both experimental and theoretical methods. It is well established that O is the most favored protonation site of FM. As mentioned above, the most elaborated exploration of the protonated FM in its ground S_0 state was carried out by Tortajada et al.¹⁸ using the composite G2 method. For the sake of comparison, we briefly describe the S_0 decompositions followed by the T_1 energy surface of the $(\text{CH}_3\text{NO})^+$ system.

3.3.1. Decomposition of Protonated Formamide in the Ground State. Several decompositions of protonated FM on the S_0 surface are displayed in Figure 7. Relative energies of the equilibrium and transition structures from our present calculations are given in green, whereas G2 relative energies taken from Tortajada's paper¹⁸ are given in red with smaller size for the purpose of comparison.

Earlier G2 values¹⁸ turn out to be close to the present CCSD(T)/CBS relative energies for **1H'**, **3H'**, **ts-1H,3H'**, **ts-1H'-P**, and $\text{NH}_4^+ + \text{CO}$. In the present work, alternative reaction steps via **1H'** and additional steps via **3H'** are also found and reported here. Beside the one-step reaction, transformation of **1H** to **1H'** can proceed via **1H''**. Although this alternative route has a low barrier for the first step, the TS in the rate-determining step connecting **1H''** and **1H'** has a high energy of 54.9 kcal/mol. This value is quite close to the barrier of 53.9 kcal/mol for a direct rearrangement between **1H** and **1H'**. The G2 energy of the TS directly connecting **3H'** and the product $\text{NH}_4^+ + \text{CO}$ was reported to be 80.8 kcal/mol.¹⁸ A closer observation on the optimized geometries of **3H'** points out that the position of the H atom linking to oxygen atom is not favorable for its transfer to nitrogen atom with the N–C–O–H in the trans position. Therefore, to reach the relevant TS, the H atom needs to rotate to form isomer with N–C–O–H in cis configuration **3H''** in which the H atom is closer to N. The resulting barrier of this additional step is 77.2 kcal/mol, which is marginally lower than the barrier of 80.1 kcal/mol of the hydrogen transfer reaction from **3H''** to $\text{NH}_4^+ + \text{CO}$.

In the $[\text{HNCH}]^+ + \text{H}_2\text{O}$ dehydration, the differences between CCSD(T)/CBS and G2 values for **ts-1H,2H** and the products are also quite small. However, our calculated relative energy of **ts-2H,P** is much lower than the G2 value, with an energy difference of ~11 kcal/mol. Comparison of the two optimized TS structures shows that the MP2/aug-cc-pVTZ optimized C–N distance is ~0.04 Å shorter than the MP2/6-31G(d) distance reported in ref 18. Such a difference in MP2 optimized geometries using two different basis sets is hardly the reason for the energy difference. A plausible reason is due to the variance between the quadratic configuration interaction QCISD(T) energies used in the composite G2 method with the present CCSD(T).

The final products of new reaction channels plotted in Figure 7 are put in the rectangular box with a green background. The hydronium ion elimination reaction pathway via the carbene isomer **3H** has a slightly lower barrier than the dehydrogenation. An energy barrier of 9.0 kcal/mol for formation of $\text{HNC} + \text{H}_3\text{O}^+$ from **3H** is markedly lower than those of other pathways in which **3H** is first transformed into **3H'** and then the latter follows two subsequent rearrangements to form $[\text{NH}_4]^+ + \text{CO}$.¹⁸ Dehydrogenation can be proceeded via one-step reactions to form two isomeric cations, $[\text{H}_2\text{NCO}]^+$ and $[\text{HNCOH}]^+$. The latter can be transformed into the former via $[\text{H}_2\text{NCO-ts}]^+$, but this TS is highly unstable with a barrier height of 139.1 kcal/mol, and thus this transformation is unlikely to happen.

3.3.2. Protonated Formamide and Its Isomers in the Triplet State. Three different protonation sites of FM are examined including N-protonation forming **1H'-T1**, C-protonation forming **1H*-T1**, and O-protonation forming two conformers **1H-T1** and **1H''-T1** with **1H-T1** being the most stable. Calculated proton affinities (PA) given in Table 2

Table 2. Proton Affinities (PA) in kcal/mol of Formamide Obtained at the CCSD(T)/CBS//MP2/aug-cc-pVTZ Level

PA	T_1	S_0	S_0 (exp. ⁴⁰)
1H-	196.4	198.5	198.4
1H' -	194.6	182.5	
1H''-	193.8		
1H* -	188.7		

are in agreement with available experiment⁴⁰ and numerous previous theoretical data.^{7,16,19,41} Clearly, while the T_1 PA from **1H-T1** is lower, that of **1H'-T1** is much larger than the corresponding values in the S_0 state. Such a reduction in PA difference between **1H-T1** and **1H'-T1** is consistent with the reduction in their energy difference. In the T_1 state, the 1.7 kcal/mol energy difference between **1H-T1** and **1H'-T1** forms is significantly smaller as compared to the 16.8 kcal/mol gap on the S_0 surface. As compared to the 6 kcal/mol energy difference on the S_1 surface,²¹ the N-protonated isomer is clearly more stabilized upon triplet excitation than following singlet excitation. The **1H''-T1** and **1H*-T1** forms are less stable with relative energies of 2.6 and 7.7 kcal/mol, respectively.

Figure 8 shows the unimolecular interconversions and rearrangements between different FM T_1 protonated forms. The O- and N-protonated forms of carbene isomer are now labeled as **3H-T1** and **3H'-T1**, and the O- and C-protonated forms of formimic acid as **2H'-T1** and **2H''-T1**, respectively. Similar to the stabilization of T_1 carbene isomer, triplet excitation greatly stabilizes its protonated forms (**3H-T1** and **3H'-T1**). Relative energies of **3H** and **3H'** species are 66.3 and 54.8 kcal/mol, whereas those of **3H-T1** and **3H'-T1** species are 16.4 and -2.5 kcal/mol, respectively. The N-protonated carbene (**3H'-T1**) becomes now the most stable protonated form in the T_1 state, at the expense of **1H-T1**. However, for the sake of comparison with the potential energy profiles of the S_0 protonated FM and the neutral T_1 FM, the energies of all stationary points are still relative to that of **1H-T1** taken as the reference.

The barriers for interconversion are calculated in the range of 3.1–69.4 kcal/mol. The lowest one corresponds to a conversion between two conformers **1H-T1** and **1H'-T1** and the highest one the rearrangement between **1H'-T1** and **1H''-**

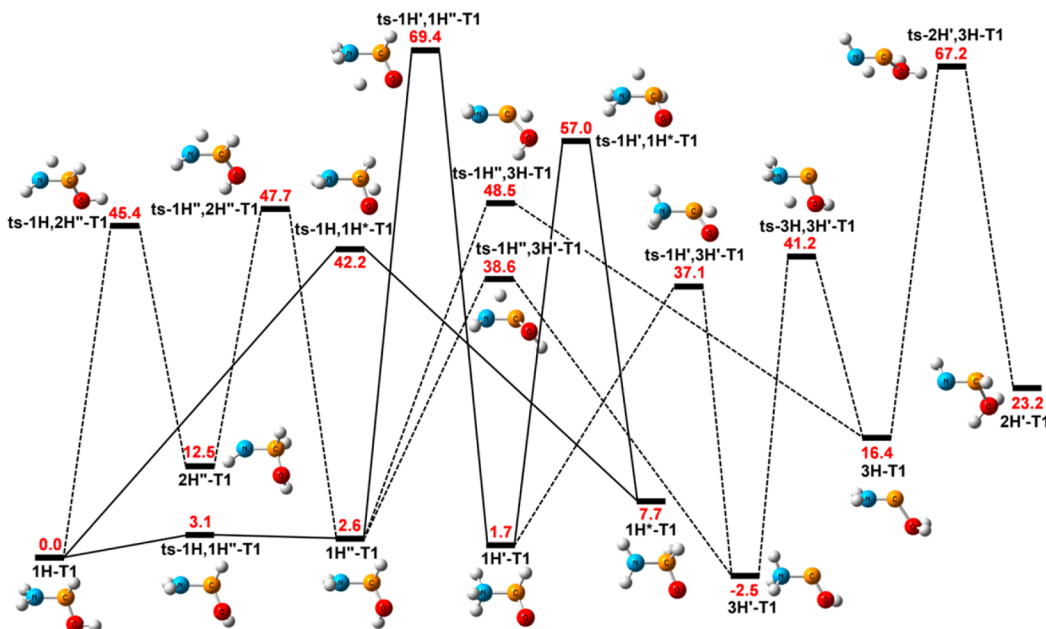


Figure 8. Schematic potential energy profiles of interconversions of protonated FM forms in the T_1 state. CCSD(T)/CBS + ZPE energies (kcal/mol) are given relative to $1H\text{-T1}$.

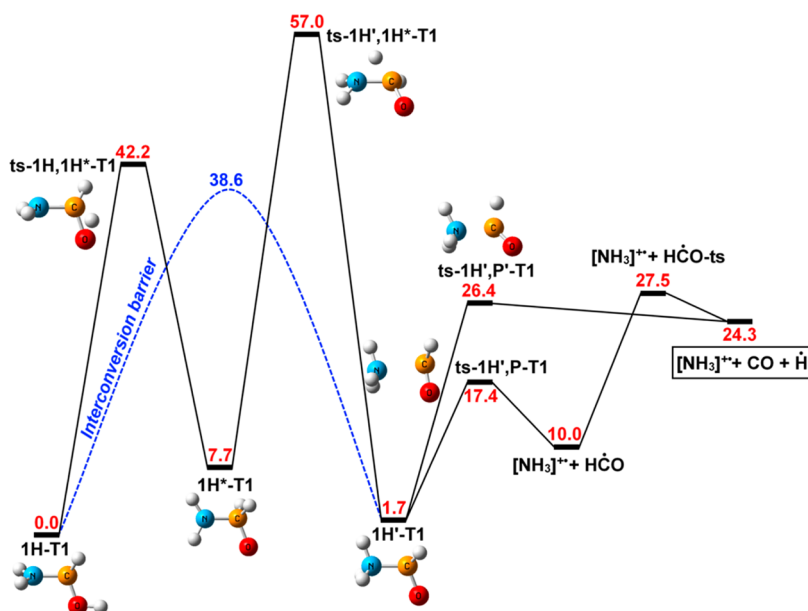


Figure 9. Schematic potential energy profiles of decarbonylation reactions of protonated formamide in the T_1 state. CCSD(T)/CBS + ZPE energies (kcal/mol) are relative to $1H\text{-T1}$.

T1. The lowest possible multistep interconversion pathways in going from $1H\text{-T1}$ to $3H\text{-T1}$, $3H'\text{-T1}$, and $1H'\text{-T1}$ all have comparable energy barriers for the rate-determining step, which amount to around 40.0 kcal/mol. The one-step interconversions from $1H\text{-T1}$ to $1H^*\text{-T1}$ and from $1H\text{-T1}$ to $2H''\text{-T1}$ are associated with energy barriers of 42.2 and 45.4 kcal/mol, respectively.

3.3.3. Reaction Pathways of Protonated Formamide on the Triplet Energy Surface. As shown in Figure 9, decarbonylation does not directly proceed from the O-protonated $1H\text{-T1}$ but rather via the N-protonated $1H'\text{-T1}$. With an energy barrier of 38.6 kcal/mol, interconversion between $1H\text{-T1}$ and $1H'\text{-T1}$ becomes the rate-determining step in the decarbonylation process from $1H\text{-T1}$. However, subsequent reaction

from $1H'\text{-T1}$ forming $\text{NH}_4^+ + \text{CO}$ is not found in the T_1 state. $1H'\text{-T1}$ can either directly dissociate into $[\text{NH}_3]^{+\bullet}$, CO , and H^\bullet , or follow two-step dissociation whose first step generates $[\text{NH}_3]^{+\bullet}$ plus HCO radical. The latter products are lower in energy and can be more easily formed from $1H'\text{-T1}$ than from the former. Therefore, it is possible that the built-up HCO radical can recombine with other available radicals, or simply dissociate to release CO with a much lower barrier.

The water complexes including $3H\text{-T1}$, $2H'\text{-T1}$, and $4R$ (Figure 10) contain each a water fragment, which possibly follows subsequent weak dissociation releasing water. The TSs located here characterizing these dehydrations are all lower in energy than the products. They are similar to the dehydration of $3H$ in the S_0 state forming $[\text{NH}_2\text{C}]^+$ product.¹⁸ Therefore,

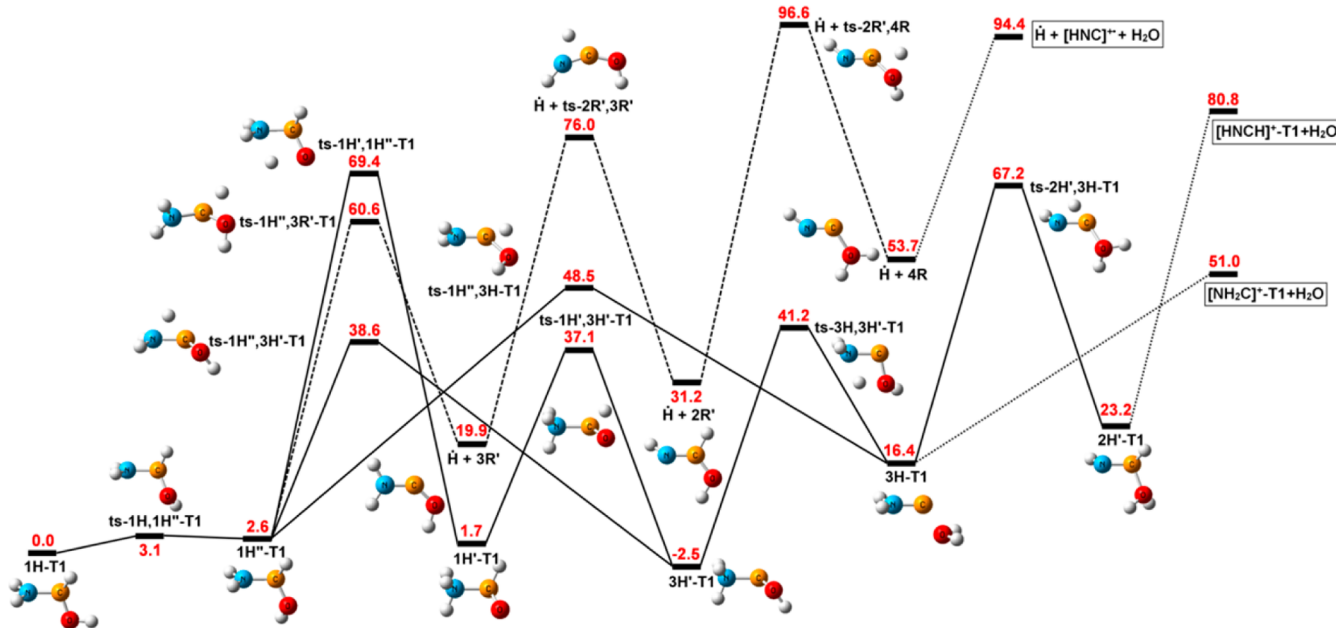


Figure 10. Schematic potential energy profiles of reaction pathways of protonated FM forming water complexes in the T_1 state. CCSD(T)/CBS + ZPE energies (kcal/mol) are given relative to **1H-T1**.

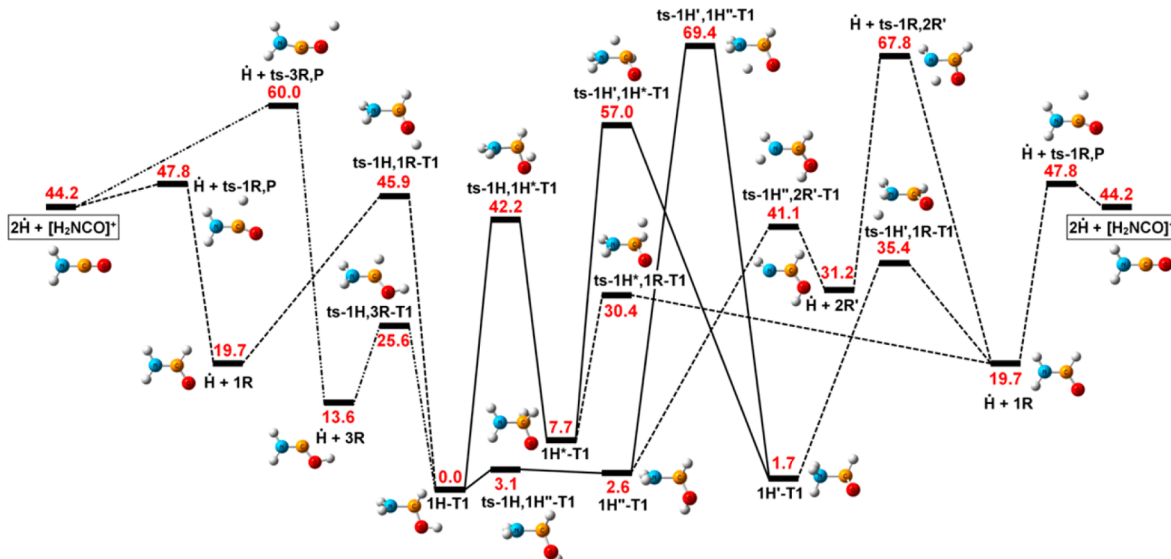


Figure 11. Schematic potential energy profiles of reaction pathways of protonated FM giving rise to $[\text{H}_2\text{NCO}]^+$ in the T_1 state. CCSD(T)/CBS + ZPE energies (kcal/mol) are relative to **1H-T1**.

the association reactions of $[\text{HNC}]^+$, $[\text{HNCH}]^+ \cdot \text{T1}$, and $[\text{NH}_2\text{C}]^+ \cdot \text{T1}$ with H_2O turn out to be all barrier-free.

For its part **1H-T1** is transformed into its **1H''-T1** conformer, which can either rearrange to form other protonated forms including **1H'-T1** and **3H'-T1** or homolytically dissociate into **3R + H[•]**. The water complex **3H-T1** can also be directly produced from **1H''-T1** via **ts-1H'',3H-T1** with a barrier of 48.5 kcal/mol. Of the different pathways generating **3H-T1**, the one involving **3H'-T1** is the lowest-lying one with a barrier of 41.2 kcal/mol for the rate-determining step. Water complex **2H'-T1** is then formed from **3H-T1** with an energy barrier of 50.8 kcal/mol. However, the very large reaction barrier and the unstable water complex product of the homolysis from **1H''-T1** make it uncompetitive.

In going from **1H-T1**, several channels are open leading to **1R**, a precursor for formation of the cation $[\text{H}_2\text{NCO}]^+$ (Figure 11). **1H-T1** can from here either follow the one-step reaction via **ts-1H,1R-T1** or rearrange into other protonated forms before dissociating. The least stable protonated form of FM (**1H*-T1**) has a large barrier for conversion from **1H-T1**. However, both interconversion and subsequent reaction forming **1R** from **1H*-T1** have barriers lower than that of the dissociation of **1R**. Having a comparable energy barrier of 47.8 kcal/mol for the rate-determining step, this reaction pathway and the one-step conversion to **1R** are the lowest possible pathways for the $[\text{H}_2\text{NCO}]^+$ product channel. Another precursor for formation of $[\text{H}_2\text{NCO}]^+$ is **3R**. Although this radical is more stable than **1R**, the relevant barrier for removal of H atom from **3R** is significantly higher than that from **1R**.

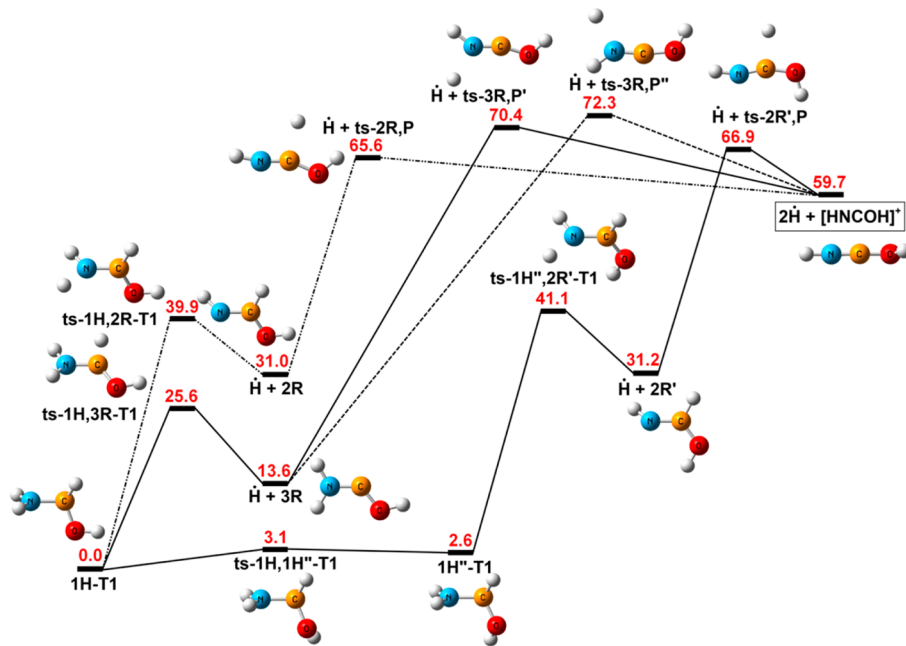


Figure 12. Schematic potential energy profiles describing reaction pathways of protonated FM leading to formation of $[\text{HNCOH}]^+$ in the T_1 state. CCSD(T)/CBS + ZPE energies (kcal/mol) are relative to 1H-T1 .

The radical 3R is also a precursor for $[\text{HNCOH}]^+$ via two TSs ($\text{ts-}3\text{R},\text{P}'$ and $\text{ts-}3\text{R},\text{P}''$, Figure 12). The latter TSs are highly unstable with the relative energies being ~ 10 kcal/mol higher than $\text{ts-}3\text{R},\text{P}$. The cation $[\text{HNCOH}]^+$ can also be formed from other radicals including 2R and $2\text{R}'$. Direct process from 1H-T1 to 2R has a barrier of 39.9 kcal/mol, which is quite close to that of the rate-determining step in the pathway forming $2\text{R}'$ through $1\text{H}''\text{-T1}$. Dissociations of both radicals 2R and $2\text{R}'$ have slightly smaller barriers than that of 3R . Dissociation from the radicals of formimic acid and carbene isomers of FM, 2R , $2\text{R}'$, and 3R , are difficult processes to achieve, with barriers in the range of 65.6–72.3 kcal/mol. These are larger than that of the dissociation 1R , which amounts to 47.8 kcal/mol.

4. CONCLUDING REMARKS

A number of new results emerge from the present theoretical study. The structures of FM and its protonated form are consistently optimized in the ground S_0 , S_1 , and T_1 states. The vertical and adiabatic excitation energies obtained using RASPT2 computations are in general close to previous experimental and theoretical data.

A strong stabilization of the carbene isomer of formamide 3-T1 and $3\text{H}'\text{-T1}$ upon triplet excitation is observed, whereas singlet excitation induces almost no effect on relative energies. The 3-T1 species is accordingly located at 7.6 kcal/mol below 1-T1 , and the formimic acid isomer 2-T1 is also 7.0 kcal/mol more stable than 1-T1 . A reversed energy ordering between isomers thus occurs following triplet transition. Protonation partially reduces the stabilization effect of triplet excitation on 3-T1 species, but the $3\text{H}'\text{-T1}$ species is still 2.5 kcal/mol lower in energy than the 1H-T1 species. For formimic acid isomer, protonation completely cancels the stabilization effect. The lowest-lying protonated form of formimic acid $2\text{H}''\text{-T1}$ is calculated to be at 12.5 kcal/mol above the 1H-T1 species. This energy difference is nearly equal to the gap between 1 and 2 on the ground state (S_0) energy surface.

Table 3. A Summary of Possible Product Channels of Neutral and Protonated Formamide Decompositions in the S_0 , S_1 , and T_1 States

state	system	products	energy barrier (kcal/mol)
S_0	$[\text{CH}_4\text{ON}]^+$	$\text{NH}_4^+ + \text{CO}$	54.9
		$[\text{HNCO}]^+ + \text{H}_2$	101.3
		$[\text{H}_2\text{NCO}]^+ + \text{H}_2$	94.4
		$[\text{HNCH}]^+ + \text{H}_2\text{O}$	59.3
S_1	$[\text{CH}_3\text{ON}]$	$^*\text{NH}_2 + ^*\text{HCO}$	15.5
		$^*\text{NH}_2 (S_1) + \text{H}^+ + \text{CO}$	61.2
		$^*\text{HNCHO} + \text{H}^+$	32.3
		$^*\text{H}_2\text{NCO} + \text{H}^+$	35.7
		$\text{HCN} (S_1) + \text{H}_2\text{O}$	74.1
		$\text{HNC} (S_1) + \text{H}_2\text{O}$	78.3
		$^*\text{NH}_2 + ^*\text{HCO}$	4.5
T_1	$[\text{CH}_3\text{ON}]$	$^*\text{NH}_2 + \text{H}^+ + \text{CO}$	13.7
		$\text{NH}_3 (T_1) + \text{CO}$	31.3
		$^*\text{HNCHO} + \text{H}^+$	28.5
		$^*\text{H}_2\text{NCO} + \text{H}^+$	8.3
		$\text{HNCO} + 2\text{H}^+$	25.8
		$\text{HCN} (T_1) + \text{H}_2\text{O}$	50.5
		$\text{HNC} (T_1) + \text{H}_2\text{O}$	61.0
		$[\text{NH}_3]^{*+} + ^*\text{HCO}$	38.6
		$[\text{NH}_3]^{*+} + \text{CO} + \text{H}^+$	38.6
		$[\text{HNCOH}]^+ + 2\text{H}^+$	65.6
T_1	$[\text{CH}_4\text{ON}]^+$	$[\text{H}_2\text{NCO}]^+ + 2\text{H}^+$	47.8
		$[\text{HNCH}]^+ (T_1) + \text{H}_2\text{O}$	67.2
		$[\text{H}_2\text{NC}]^+ (T_1) + \text{H}_2\text{O}$	41.2
		$[\text{HNC}]^{*+} + \text{H}^+ + \text{H}_2\text{O}$	96.6

Possible decomposition pathways of both the neutral and the protonated formamide in the low-lying excited states are explored using different levels of theory. The main characteristics are summarized in Table 3. In the excited S_1 and T_1 states, FM tends to follow C–N homolytic bond dissociations forming the $\text{NH}_2 + \text{HCO}$ radical pair.

The HCN and HNC molecules can be formed from both neutral and protonated FM in the ground and excited states via multistep dehydration pathways. Because of the stabilization effect of triplet excitation, the barriers for the dehydration reaction pathways on the T_1 state turn out to be lower than those on the S_0 and S_1 states. The lowest possible reaction pathway forming HCN is found on the T_1 energy surface that has the energy barrier of 50 kcal/mol, which is 23 kcal/mol lower than that on the ground S_0 surface. Upon protonation, the barrier for this pathway on the T_1 state tends to increase to 66 kcal/mol, which is also lower than the corresponding value of >80 kcal/mol on the S_0 surface. Dehydration pathways on the singlet excited S_1 surface also have very large energy barriers, which amount to 74 and 78 kcal/mol for formation of HCN and HNC, respectively. In addition, preferred products are the relatively stable water complexes. This is also observed for dehydration pathway of protonated FM in the T_1 state. Overall, although the most favorable pathway for formation of HCN/HNC is the dehydration of FM in the T_1 state, this reaction mode is not competitive with homolytic C–N bond cleavages that ultimately give rise to formation of CO.

ASSOCIATED CONTENT

Supporting Information

Cartesian coordinates, harmonic vibrational frequencies, and rotational constants of structures considered in this work. This material is available free of charge via the Internet at <http://pubs.acs.org>.

AUTHOR INFORMATION

Corresponding Author

*Fax: +32-16-327992. E-mail: minh.nguyen@chem.kuleuven.be.

Notes

The authors declare no competing financial interest.

ACKNOWLEDGMENTS

We are grateful to Ria Broer at the University of Groningen, The Netherlands, for her interest and support. We also thank Thom Orlando at Georgia Institute of Technology, Atlanta, GA, for valuable discussion on prebiotic chemistry within the framework of the NASA-NSF Center for Chemical Evolution. H.T.N. received a doctoral scholarship from an interdisciplinary research project (IDO-2011) of KU Leuven on Exoplanets. R.W.A.H. acknowledges the Zernike Institute for Advanced Materials for financial support (“Dieptestrategie” program).

REFERENCES

- (1) Saladino, R.; Crestini, C.; Pino, S.; Costanzo, G.; Di Mauro, E. Formamide and the Origin of Life. *Phys. Life Rev.* **2012**, *9*, 84–104.
- (2) Nguyen, V. S.; Abbott, H. L.; Dawley, M. M.; Orlando, T. M.; Leszczynski, J.; Nguyen, M. T. Theoretical Study of Formamide Decomposition Pathways. *J. Phys. Chem. A* **2011**, *115*, 841–851.
- (3) Lundell, J.; Krajewska, M.; Räsänen, M. Matrix Isolation Fourier Transform Infrared and Ab Initio Studies of the 193-nm-Induced Photodecomposition of Formamide. *J. Phys. Chem. A* **1998**, *102*, 6643–6650.
- (4) Liu, D.; Fang, W.-H.; Fu, X.-Y. Ab Initio Molecular Orbital Study of the Mechanism of Photodissociation of Formamide. *Chem. Phys. Lett.* **2000**, *318*, 291–297.
- (5) Kang, T.; Kim, H. Photodissociation of Formamide at 205 nm: The H Atom Channels. *Chem. Phys. Lett.* **2006**, *431*, 24–27.
- (6) Antol, I.; Eckert Maksic, M.; Barbatti, M.; Lischka, H. Simulation of the Photodeactivation of Formamide in the $n(O)-\pi^*$ and $\pi-\pi^*$ States: An Ab Initio On-the-Fly Surface-Hopping Dynamics Study. *J. Chem. Phys.* **2007**, *127*, 234303–234306.
- (7) Antol, I.; Barbatti, M.; Eckert Maksic, M.; Lischka, H. Quantum Chemical Calculations of Electronically Excited States: Formamide, its Protonated Form and Alkali Cation Complexes as Case Studies. *Monatsh. Chem.* **2008**, *139*, 319–328.
- (8) Antol, I.; Vazdar, M.; Barbatti, M.; Eckert Maksic, M. The Effect of Protonation on the Photodissociation Processes in Formamide - An Ab Initio Surface Hopping Dynamics Study. *Chem. Phys.* **2008**, *349*, 308–318.
- (9) Ferus, M.; Kubelik, P.; Civis, S. Laser Spark Formamide Decomposition Studied by FT-IR Spectroscopy. *J. Phys. Chem. A* **2011**, *115*, 12132–12141.
- (10) Saladino, R.; Crestini, C.; Cossetti, C.; Di Mauro, E.; Deamer, D. Catalytic effects of Murchison Material: Prebiotic Synthesis and Degradation of RNA Precursors. *Origins Life Evol. Biospheres* **2011**, *41*, 437–451.
- (11) Nguyen, V. S.; Orlando, T. M.; Leszczynski, J.; Nguyen, M. T. Theoretical Study of the Decomposition of Formamide in the Presence of Water Molecules. *J. Phys. Chem. A* **2013**, *117*, 2543–2555.
- (12) (a) Wang, J.; Gu, J.; Nguyen, M. T.; Springsteen, G.; Leszczynski, J. From Formamide to Purine: An Energetically Viable Mechanistic Reaction Pathway. *J. Phys. Chem. B* **2013**, *117*, 2314–2320. (b) Wang, J.; Gu, J.; Nguyen, M. T.; Springsteen, G.; Leszczynski, J. From Formamide to Purine: a Self-Catalyzed Reaction Pathway Provides a Feasible Mechanism for the Entire Process. *J. Phys. Chem. B* **2013**, *117*, in press.
- (13) Boden, J. C.; Back, R. A. Photochemistry and Free-Radical Reactions in Formamide Vapour. *Trans. Faraday Soc.* **1970**, *66*, 175–182.
- (14) Krug, J. P.; Popelier, P. L. A.; Bader, R. F. W. Theoretical Study of Neutral and of Acid and Base-Promoted Hydrolysis of Formamide. *J. Phys. Chem.* **1992**, *96*, 7604–7616.
- (15) Lin, H.-Y.; Ridge, D. P.; Uggerud, E.; Vulpius, T. Unimolecular Chemistry of Protonated Formamide. Mass Spectrometry and ab Initio Quantum Chemical Calculations. *J. Am. Chem. Soc.* **1994**, *116*, 2996–3004.
- (16) Ou, M.-C.; Chu, S.-Y. Protonation Sites and Rotational Barriers Calculation for Formamide and Thioformamide. *J. Phys. Chem.* **1995**, *99*, 556–562.
- (17) Pranata, J.; Davis, G. D. Computational Investigations of Reactive Intermediates in the Acid-Catalyzed Proton Exchange in Formamide. *J. Phys. Chem.* **1995**, *99*, 14340–14346.
- (18) Tortajada, J.; Leon, E.; Morizur, J. P.; Luna, A.; Mo, O.; Yanez, M. Potential Energy Surface of Protonated Formamide and of Formamide-X+ (X = Li, Na, Mg, and Al) Complexes. *J. Phys. Chem.* **1995**, *99*, 13890–13898.
- (19) Bagno, A.; Scorrano, G. Site of Ionization of Polyfunctional Bases and Acids. I. Ab Initio Proton Affinities. *J. Phys. Chem.* **1996**, *100*, 1536–1544.
- (20) Cho, S. J.; Cui, C.; Lee, J. Y.; Park, J. K.; Suh, S. B.; Park, J.; Kim, B. H.; Kim, K. S. N-Protonation vs O-Protonation in Strained Amides: Ab Initio Study. *J. Org. Chem.* **1997**, *62*, 4068–4071.
- (21) Antol, I.; Eckert Maksic, M.; Lischka, H. Ab Initio MR-CISD Study of Gas-Phase Basicity of Formamide in the First Excited Singlet State. *J. Phys. Chem. A* **2004**, *108*, 10317–10325.
- (22) Olsen, J.; Roos, B. O.; Jorgensen, P.; Jensen, H. J. A. Determinant Based Configuration Interaction Algorithms for Complete and Restricted Configuration Interaction Spaces. *J. Chem. Phys.* **1988**, *89*, 2185–2192.
- (23) Malmqvist, P. A.; Rendell, A.; Roos, B. O. The Restricted Active Space Self-Consistent-Field Method, Implemented with a Split Graph Unitary Group Approach. *J. Phys. Chem.* **1990**, *94*, 5477–5482.
- (24) Celani, P.; Werner, H.-J. Multireference Perturbation Theory for Large Restricted and Selected Active Space Reference Wave Functions. *J. Chem. Phys.* **2000**, *112*, 5546–5557.
- (25) Peterson, K. A.; Woon, D. E.; Dunning, J. T. H. Benchmark Calculations with Correlated Molecular Wave Functions. IV. The

- Classical Barrier Height of the H+H₂ → H₂+H Reaction. *J. Chem. Phys.* **1994**, *100*, 7410–7415.
- (26) Gaussian 09, revision A.02; Gaussian, Inc.: Wallingford, CT, 2009.
- (27) Fogarasi, G.; Szalay, P. G. High-Level Electron Correlation Calculations on Formamide and the Resonance Model. *J. Phys. Chem. A* **1997**, *101*, 1400–1408.
- (28) Krauss, M.; Webb, S. P. Solvation and the Excited States of Formamide. *J. Chem. Phys.* **1997**, *107*, 5771–5775.
- (29) Li, Y.; Garrell, R. L.; Houk, K. N. Mechanism of Cis-Trans Isomerizations of Amide and Peptide Excited States. *J. Am. Chem. Soc.* **1991**, *113*, 5895–5896.
- (30) Gingell, J. M.; Mason, N. J.; Zhao, H.; Walker, I. C.; Siggel, M. R. F. VUV Optical-Absorption and Electron-Energy-Loss Spectroscopy of Formamide. *Chem. Phys.* **1997**, *220*, 191–205.
- (31) Besley, N.; Doltsinis, N. Ab Initio Finite-Temperature Electronic Absorption Spectrum of Formamide. *J. Chem. Theory Comput.* **2006**, *2*, 1598–1604.
- (32) Chong, D. Density Functional Theory Study of The Electron Spectra of Formamide Vapor. *J. Electron Spectrosc.* **2011**, *184*, 164–169.
- (33) Serrano-Andrés, L.; Fülscher, M. P. Theoretical Study of the Electronic Spectroscopy of Peptides. 1. The Peptidic Bond: Primary, Secondary, and Tertiary Amides. *J. Am. Chem. Soc.* **1996**, *118*, 12190–12199.
- (34) Harding, L. B.; Goddard, W. A. Generalized Valence Bond Description of the Valence States of Formamide. *J. Am. Chem. Soc.* **1975**, *97*, 6300–6305.
- (35) Ha, T.-K.; Keller, L. Ab Initio SCF and CI Study of the Electronic Structure and the n → π* Excitation of CH₃CHO, NH₂CHO, HOCHO and FCHO. *J. Mol. Struct.* **1975**, *27*, 225–232.
- (36) Stenkamp, L. Z.; Davidson, E. R. An Ab Initio Study of Formamide. *Theor. Chem. Acc.* **1977**, *44*, 405–419.
- (37) Staley, R. H.; Harding, L. B.; Goddard III, W. A.; Beauchamp, J. L. Triplet States of the Amide Group. Trapped Electron Spectra of Formamide and Related Molecules. *Chem. Phys. Lett.* **1975**, *36*, 589–593.
- (38) Bouchoux, G.; Espagne, A. Ionized Aminohydroxycarbene and its Isomers: Relative Stability and Unimolecular Reactivity. *Chem. Phys. Lett.* **2001**, *348*, 329–336.
- (39) Back, R. A.; Boden, J. C. High-Temperature Photolysis and the Pyrolysis of Formamide Vapour, and the Thermal Decomposition of the Carbamyl Radical. *Trans. Faraday Soc.* **1971**, *67*, 88–96.
- (40) Lias, S. G.; Liebman, J. F.; Levin, R. D. Evaluated Gas Phase Basicities and Proton Affinities of Molecules; Heats of Formation of Protonated Molecules. *J. Phys. Chem. Ref. Data* **1984**, *13*, 695–808.
- (41) Moisan, S.; Dannenberg, J. J. Molecular Orbital Calculations on the Protonation of Hydrogen-Bonded Formamide Chains. Implications for Peptides. *J. Phys. Chem. B* **2003**, *107*, 12842–12846.